



Article

Prediction of Stem Water Potential in Olive Orchards Using High-Resolution Planet Satellite Images and Machine Learning Techniques

Simone Pietro Garofalo ^{1,*}, Vincenzo Giannico ¹, Leonardo Costanza ¹, Salem Alhajj Ali ¹, Salvatore Camposeo ¹, Giuseppe Lopriore ¹, Francisco Pedrero Salcedo ² and Gaetano Alessandro Vivaldi ¹

¹ Department of Soil, Plant and Food Science, University of Bari Aldo Moro, Via Amendola 165/A, 70126 Bari, Italy; vincenzo.giannico@uniba.it (V.G.); leonardo.costanza@uniba.it (L.C.); salem.alhajj@uniba.it (S.A.A.); salvatore.camposeo@uniba.it (S.C.); giuseppe.lopriore@uniba.it (G.L.); gaetano.vivaldi@uniba.it (G.A.V.)

² Department of Irrigation, CEBAS-CSIC, Campus Universitario de Espinardo, 30100 Murcia, Spain; fpedrero@cebas.csic.es

* Correspondence: simone.garofalo@uniba.it

Abstract: Assessing plant water status accurately in both time and space is crucial for maintaining satisfactory crop yield and quality standards, especially in the face of a changing climate. Remote sensing technology offers a promising alternative to traditional in situ measurements for estimating stem water potential (Ψ_{stem}). In this study, we carried out field measurements of Ψ_{stem} in an irrigated olive orchard in southern Italy during the 2021 and 2022 seasons. Water status data were acquired at midday from 24 olive trees between June and October in both years. Reflectance data collected at the time of Ψ_{stem} measurements were utilized to calculate vegetation indices (VIs). Employing machine learning techniques, various prediction models were developed by considering VIs and spectral bands as predictors. Before the analyses, both datasets were randomly split into training and testing datasets. Our findings reveal that the random forest model outperformed other models, providing a more accurate prediction of olive water status ($R^2 = 0.78$). This is the first study in the literature integrating remote sensing and machine learning techniques for the prediction of olive water status in order to improve olive orchard irrigation management, offering a practical solution for estimating Ψ_{stem} avoiding time-consuming and resource-intensive fieldwork.



Citation: Garofalo, S.P.; Giannico, V.; Costanza, L.; Alhajj Ali, S.; Camposeo, S.; Lopriore, G.; Pedrero Salcedo, F.; Vivaldi, G.A. Prediction of Stem Water Potential in Olive Orchards Using High-Resolution Planet Satellite Images and Machine Learning Techniques. *Agronomy* **2024**, *14*, 1. <https://doi.org/10.3390/agronomy14010001>

Academic Editor: Valerio Cristofori

Received: 23 November 2023

Revised: 15 December 2023

Accepted: 17 December 2023

Published: 19 December 2023



Copyright: © 2023 by the authors. Licensee MDPI, Basel, Switzerland. This article is an open access article distributed under the terms and conditions of the Creative Commons Attribution (CC BY) license (<https://creativecommons.org/licenses/by/4.0/>).

1. Introduction

The Mediterranean basin is famous for its rich history of olive tree cultivation since the Roman and Greek civilizations [1], both for table olives and olive oil production, which represent essential components of the Mediterranean diet [2]. The climate condition in these areas is generally characterized by hot summers and mild winters, which are well-suited for olive tree growth [3]. According to the International Olive Oil Council [4], Mediterranean countries accounted for approximately 97% of the world's olive cultivation, with countries such as Spain, Italy, Portugal, Greece, and France being the leaders in global olive production, representing 81% of the total olive production [2]. In addition to their economic value, olive agroecosystems have a long-lasting history and represent an invaluable local heritage for landscape, trade, and social traditions [5], sometimes cultivated as a part of agroforestry systems [6]. Most of the olive-growing areas of the Mediterranean region are located in a semi-arid environment with high annual ET_o and low annual rainfall. The general trends for fresh water supply limitations in Mediterranean countries make it essential to understand the olive tree water relations [7], as well as to develop measurement methods for olive tree water status and stress detection in large

areas [8]. It is widely accepted that water deficiencies can lead to significant yield loss, whereas adequate management of irrigation water can optimize crop production as well as the fruit quality (technological, nutraceutical, and health) of the extra virgin olive oil obtained [9]. Moreover, reducing water supplies in the most drought-tolerant phenological phases does not decrease fruit yield, accelerate fruit maturity, and improve the polyphenols content of the olive oil [10].

It has always been believed that plant water requirements differ among species and even cultivars, making irrigation scheduling and management a complex task for growers [11]. Therefore, site- or crop-specific water status monitoring is becoming crucial to optimize irrigation scheduling [12]. Traditionally, *in situ* measurements of plant water status are labor-intensive, time-consuming, and destructive, allowing only limited samples and repetitions. Therefore, reliable measurements of plant water stress over large areas are often required for water management applications in agriculture. Remote sensing has increasingly been utilized to detect plant water stress, with interesting advantages, e.g., cost-effectiveness and versatility, leading to a useful spatial display of the water stress patterns necessary to manage orchard irrigation [13]. Various vegetation indices have been related to leaf and canopy water content [13]. Leaf water potential (Ψ_{leaf}) measurements can detect the onset of water deficiency, allowing a reaction before permanent damage occurs [14]. However, it can result in high variability within one tree. Recent studies regarding irrigation water scheduling and management have focused on the stem water potential (Ψ_{stem}) as an important parameter of the water status of non-transpiring leaves, which is related to water availability and transpiration. To solve the problem of water status variability within one tree, most researchers focused on the measurement of Ψ_{stem} as an indicator of plant water status in several fruit orchards [14–16], including olive trees, for which Ψ_{stem} measurement is crucial for irrigation planning and scheduling [17,18]. Nevertheless, there is little information in the literature regarding irrigation strategies using Ψ_{stem} in olive trees [19] due to the lack of reliable methodology for continuous and economically viable monitoring of Ψ_{stem} in different olive orchard environments. Although numerous works are showing the usefulness of monitoring some physiological parameters such as Ψ_{stem} [20] and stomatal conductance [21] in an open field (using proximal sensors) for the correct water irrigation management and to optimize water use efficiency in olive cultivation, the potential of remote monitoring of Ψ_{stem} , using different remote sensing (RS) platforms, has not yet been fully explored nor widely adopted [22], especially in olive orchards. Recent studies by Caruso et al. [18,22] for the estimation of some physiological parameters based on images acquired by UAVs showed the benefits of RS technology in terms of simplifying the data acquisition, which is useful for irrigation management. Nevertheless, the use of UAVs is still expensive and needs extensive fieldwork to operate them. A previous study by Suárez et al. [23] used a series of diurnal airborne campaigns by Airborne Hyperspectral Scanner (AHS) over two years in an olive orchard field to investigate changes in the canopy photochemical reflectance index (PRI), the combined TCARI/OSAVI, and normalized difference vegetation index (NDVI), as an indicator of water stress, as a function of field-measured physiological indicators of water stress such as stomatal conductance, stem water potential, steady-state fluorescence, and the canopy crown's temperature. Among the three VIs calculated, the authors found that only the airborne PRI demonstrated sensitivity to diurnal changes in physiological indicators of water stress, including Ψ_{stem} measured in the field at the time of each image acquisition. However, the use of airplanes is still time-consuming and can add significant costs to farmers due to their operational costs. Therefore, using satellite images to estimate plant water status parameters would be a viable option as a rapid data acquisition source. In this study, remote sensing data were acquired from commercial smallsats, specifically Planet's PlanetScope sensors [24], and processed in QGIS [25] to obtain the reflectance value of each spectral band and to calculate vegetation indices. The reflectance value of each band and the vegetation indices were used to test different machine-learning models to predict stem water potential for olive trees. The main objective of this study was to develop,

through the integration of remote sensing and machine learning techniques, a predictive model of olive orchards' water status to support farmers in managing irrigation water, reducing expensive, difficult, and time-consuming fieldwork in the frame of sustainable water irrigation management.

2. Materials and Methods

2.1. Study Site and Climatic Conditions

This study was conducted in a commercial olive orchard situated near Gallipoli (Apulia Region, Southern Italy) (latitude: $40^{\circ}01'23.3''$ N; longitude: $18^{\circ}03'06.4''$ E; 23 m above sea level) over two years (2021 and 2022). Olive trees at the study site were planted with *Olea europaea* L. cv. Leccino at a spacing of 7 m \times 7 m between rows and between trees, covering a study area of about 0.80 ha (Figure 1). The studied olive orchard was fertilized using commercial fertilizer with N 70 kg/ha—P₂O₅ 40 kg/ha—K₂O 60 kg/ha according to the regional guidelines [26] for sustainable crop management given by the local government of the Apulia Region.

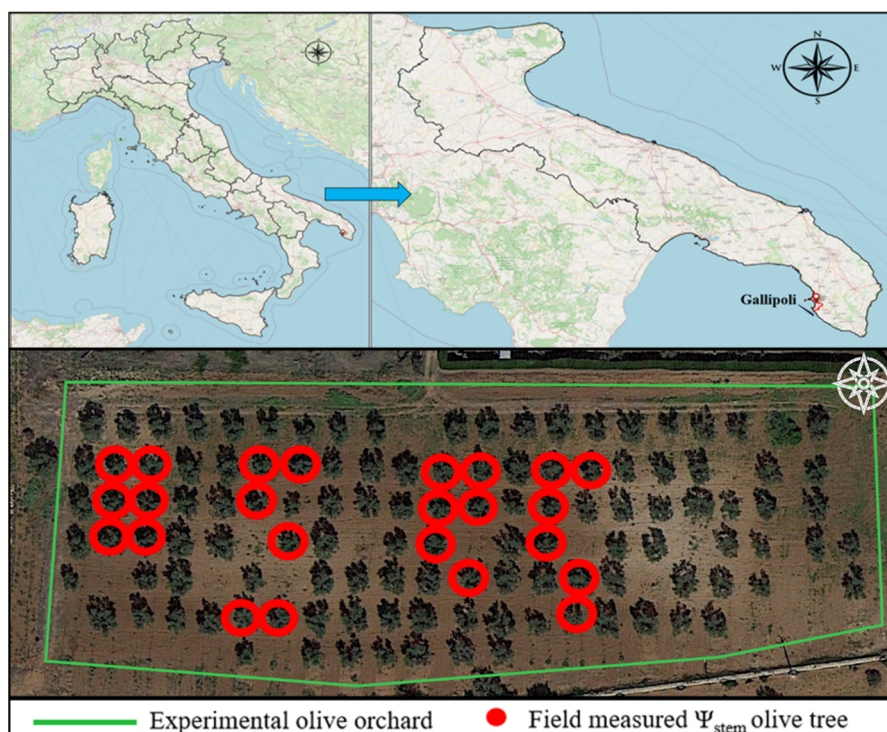


Figure 1. Location of the olive orchard experimental field. Red points indicate Ψ_{stem} measurements on the selected olive tree during the two study years (2021 and 2022) (Google Earth image ©).

The climate condition at the studied olive orchard is Mediterranean, belonging to a temperate-dry-hot summer climate-Csa class according to Köppen and Geiger, with hot and dry summers and mildly cold winters [27]. Generally, the hottest month at the study site is August (the average temperature is around 26.4°C), and the average annual rainfall is about 678 mm. Climate data during the two years were provided by the Apulia Region meteorological stations [28]. The analysis of climate data indicates that the amount of rainfall in both years was reported to be 415.4 mm and 579 mm during 2021 and 2022, respectively. However, the rainfall amount in both years was less than the annual average amount typical of the area (678 mm). In the 2021 season, the highest average temperature was reported in August (32.6°C), whereas the lowest average temperature was reported in January (8.2°C), and the rainiest month was November (123.2 mm). In the 2022 season, the highest average temperature was reported in August (32.9°C), and the lowest average temperature was reported in January (7.2°C), with the rainiest month reported to be in

December (120.9 mm). The highest values of actual evapotranspiration (ETo) were recorded in June and July in both years (Figure 2; Tables S1 and S2).

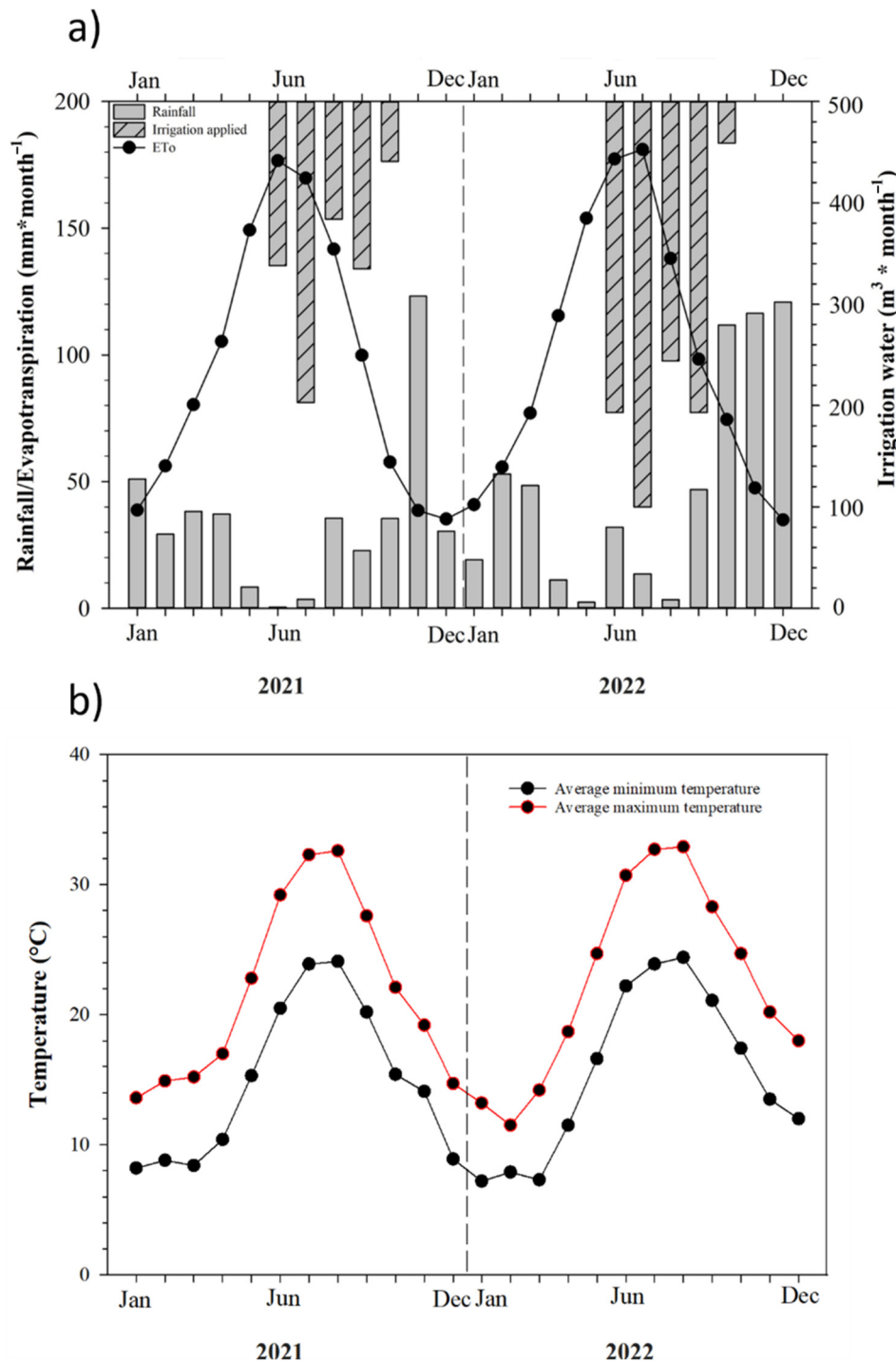


Figure 2. The monthly amount of rainfall, irrigation water applied, and trend of ETo were calculated following the Hargreaves–Samani equation [29] (a). The monthly trend of average minimum and maximum temperatures in the study area during the two years of the experiment (b).

2.2. Irrigation Management and Plant Water Status Determination

In both seasons (2021 and 2022), irrigation water in the experimental olive orchard was managed using a decision support system (DSS). Irrigation scheduling was organized to keep the soil water content (SWC) of the first 30 cm (active root zone) of the soil at an optimum level (set as a recharge point (RP) where water can be easily taken up by the plant).

This was possible by identifying the field capacity and the wilting point according to the specific physical soil characteristics of the study site. Each year, irrigation interventions were applied in full irrigation (FI) regimes scheduling, considering the differences in water needs as the crop grows, according to the phenological stages. The soil moisture was kept at 34% θ, while RP was set to 26%. Soil moisture was monitored using sensors (TEROS 12 Advanced; Meter Group, 2365 NE Hopkins Ct., Pullman, WA, USA) and a control unit (ZL6 Advanced Cloud data logger; Meter Group, 2365 NE Hopkins Ct., Pullman, WA, USA). The amount of irrigation water applied in 2021 was 799 m³; in 2022, it was 1311 m³ (Table S3). The olive orchard was irrigated more in 2022 than in 2021, considering the fruit load (in 2021, there was no production, whereas in 2022, production was about 800 kg/ha). Figure 2 reports the monthly amount of irrigation water applied and rainfall and the trend of ET₀ in both years. The salinity of the water used for irrigation was adequate (2.11 ± 0.30 dS/m), not exceeding the threshold value of 4.2 dS/m, as reported in Pedrero et al. [30]. Plant water status was measured in both years on 24 sample olive trees by detecting the stem water potential (Ψ_{stem} ; MPa) using a pressure chamber (Plant Water Status Console 3000F01, SOILMOISTURE CORP., Santa Barbara, CA, USA). However, before the measurement of Ψ_{stem} , mature and fully expanded leaves were placed in aluminum foil for 60 min. Hence, every shoot was placed in the pressure chamber, and gaseous nitrogen was insufflated until the equilibrium was reached; then, the water potential value was read on the console. In each year, Ψ_{stem} was measured 4 times during the irrigation season (from June to October; in both years, all Ψ_{stem} measurements were conducted at midday (11.00 to 13.00 h solar time)).

2.3. Satellite Data, Image Processing, and Vegetation Indices

In this study, we used PlanetScope (PS) high-resolution satellite images (Imagery© 2021 and 2022, Planet Labs PBC, San Francisco, CA, USA [24]). The PS constellation, consisting of more than 130 satellites, currently includes three generations of satellites, including SuperDoves (PSB.SD). PSB.SD is the third generation of PlanetScope sensors, which acquire daily imagery utilizing 8 spectral bands (i.e., Coastal Blue, 431–452 nm, Blue, 465–515 nm, Green I, 513–549 nm, Green, 547–583 nm, Yellow, 600–620 nm, Red, 650–680 nm, Red Edge, 697–713 nm and NIR, 845–885 nm) with a spatial resolution of 3 m and the equator crossing time of 7.30–11.30 a.m. (local solar time) [24,31]. In this study, 8 PlanetScope images were downloaded from the online tool “Planet Explorer” as orthorectified and radiometrically corrected TIFFs [24] on the same days as Ψ_{stem} field measurement. We used a spectral image acquired from a UAV at the beginning of the 2019 irrigation season to identify the trees under consideration within the field. For each tree considered, we calculated the average reflectance of the pixels—within the same spectral band—in the correspondence of the tree canopy by using the QGIS tool “Zonal statistics” (QGIS Białowieża, 3.22.5 for Windows). Additionally, several vegetation indices (VIs) were calculated: normalized difference vegetation index (NDVI), optimized soil adjusted vegetation index (OSAVI), transformed chlorophyll absorption reflectance index (TCARI), combined TCARI/OSAVI, enhanced vegetation index (EVI), modified chlorophyll absorption reflectance index (MCARI), combined MCARI/OSAVI, simple ratio (SR), transformed vegetation index (TVI), and normalized difference red edge (NDRE). The full range of the VIs calculated in this study can be seen in Table 1, along with their description and application references in olive orchards.

Table 1. Formulation and source of the vegetation indices (VIs) used in this study.

Vegetation Index (VI)	VI Full Name	Formula	Reference
NDVI	Normalized Difference Vegetation Index	$(r\text{NIR} - r\text{RED}) / (r\text{NIR} + r\text{RED})$	[32]
OSAVI	Optimized Soil Adjusted Vegetation Index	$(1 + 0.16)(r\text{NIR} - r\text{RED}) / (r\text{NIR} + r\text{RED} + 0.16)$	[33]

Table 1. Cont.

Vegetation Index (VI)	VI Full Name	Formula	Reference
TCARI	Transformed Chlorophyll Absorption Reflectance Index	$3[(rRE - rRED) - 0.2(rRE - rGREEN)(rRE/rRED)]$	[34]
TCARI/OSAVI	Combined TCARI/OSAVI	TCARI/OSAVI	[35]
EVI	Enhanced Vegetation Index	$2.5 \times [(rNIR - rRED)/(rNIR + 6 \times rRED - 7.5 \times rBLUE + 1)]$	[36,37]
MCARI	Modified Chlorophyll Absorption Reflectance Index	$[(rRE - rRED) - 0.2(rRE - rGREEN)](rRE/rRED)$	[34]
MCARI/OSAVI	Combined MCARI/OSAVI	MCARI/OSAVI	[35]
SR	Simple Ratio	$rRED/rNIR$	[38]
TVI	Transformed Vegetation Index	$\sqrt{((NDVI) + 0.5)}$	[38]
NDRE	Normalized Difference Red Edge	$(rNIR - rRE)/(rNIR + rRE)$	[39]

2.4. Statistical Analysis and Machine Learning

In this study, the performances of two machine learning techniques (support vector machine (SVM) and random forest (RF)) and linear regression (multiple linear regression (MLR)) were tested to create Ψ_{stem} predictive models and test their robustness. The first approach used was the SVM [40,41]. To test the performance of the SVM, a radial basis kernel was used by applying a tune grid-search with the function `tune()` ("e1071" package) to test different combinations of cost and gamma. The best combination found for our datasets was cost = 1.5; gamma = 1 and cost = 1.5; gamma = 0.5 for PBs and VIs, respectively. The second approach used was the MLR. In this approach, we avoided using all the variables to predict Ψ_{stem} , maintaining only the statistically significant ($p < 0.05$) variables. The third modeling was the RF [42], an ensemble learning technique. In this study, the RF models were implemented using the "ranger" package. Moreover, to optimize the performance of the models, we utilized the "caret" package. In the ranger implementation of RF, we fine-tuned several parameters, including the number of trees, the number of variables to potentially split each node (`mtry`), the splitting rule, and the minimum node size. Model calibration was run multiple times using various combinations of these parameters, except for the number of trees, which was fixed at 500, as it did not significantly impact the overall performance of the models. To evaluate the importance of each variable, we used a permutation method [43], where the increase in model prediction error was calculated for each run with one variable excluded from the predictors set. The resulting values were then scaled from 0 to 100. Pearson's r of the correlation, coefficient of determination (R^2), root mean square error (RMSE), normalized root mean square error (nRMSE), and mean absolute error (MAE) were used as measures of the performance to compare the models. The statistical analysis and modeling were performed using Rstudio (Rstudio, PBC, Boston, MA, USA) for Windows, Version 2022.12.0 + 353. For the graphical representation of information and data, SigmaPlot (SigmaPlot, Systat Software Inc., Version 14 for Windows) was used.

Data Handling

The analyses were conducted using two distinct approaches to data handling. In the first approach, data collected during the two years of the experiment were combined in a unique dataset ($n = 192$) and then randomly divided into a calibration (80%) and a testing (20%) dataset. The training dataset was used to fit the model, while the testing dataset was used to test the goodness of fit of the predictive model. In the second approach, models were trained on the first-year dataset ($n = 96$), and the performance of the models was tested on the second-year dataset ($n = 96$).

In both approaches, to predict Ψ_{stem} as a function of the variables derived from the satellite (PSB.SD), two groups of predictors were tested:

- (1) A dataset containing the PBs reflectance value for each sample tree.
- (2) A dataset containing the VIs value calculated for each sample tree.

3. Results

3.1. Stem Water Potential of Olive Trees

During the experiment, Ψ_{stem} varied over a wide range (−0.8 to about −3.5 MPa). Figure 3 shows a boxplot of Ψ_{stem} during the different phenological stages of the olive trees and in both years. The data indicates a significant variation of Ψ_{stem} between the different periods of the olive trees' development stages in both years. Figure 3 shows higher Ψ_{stem} variations over the summer period (July and August) in both years. The analysis of olives' water status results indicates that Ψ_{stem} was decreased during the fruit development (50%) phase (2021 DOY: 210; 2022 DOY: 206) and then increased during the successive phenological stages (beginning of fruit color and harvest maturity) in both years (Figure 3). Despite the variation of Ψ_{stem} across years and between crop development stages, the overall results showed that Ψ_{stem} did not fall below −4 MPa.

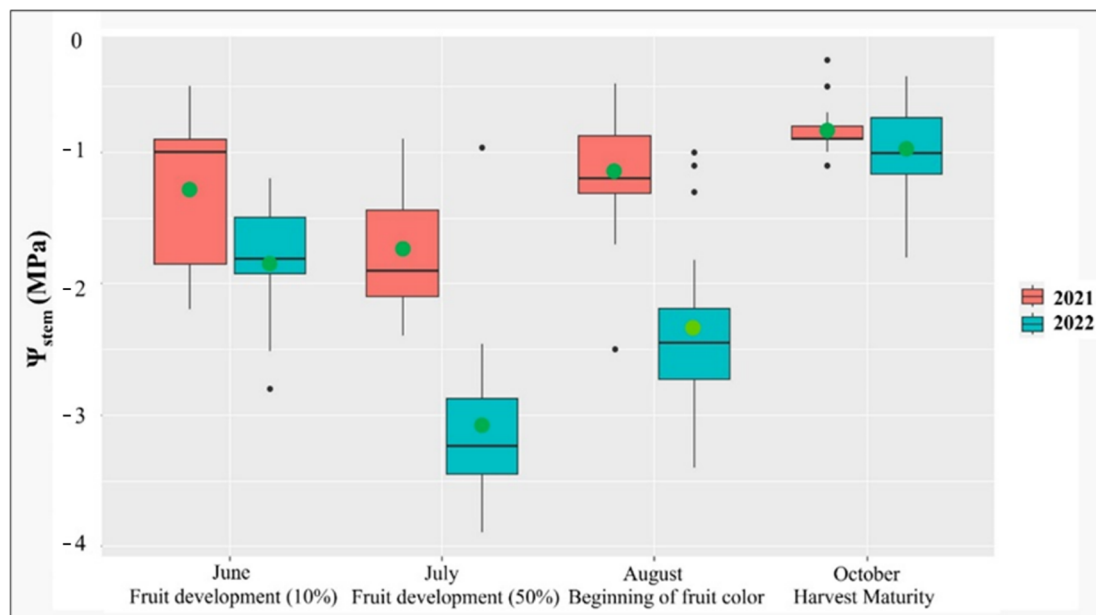


Figure 3. Box plot showing the variation of field measured Ψ_{stem} at different development stages of olive trees during both growing seasons (2021 and 2022). Green circles indicate the mean values.

3.2. Multispectral Planet Band Reflectance Value and Vegetation Indices

In this study, the ratio of the reflectance in different spectral bands was used to calculate 10 VIs (Table 1) according to the spectral characteristics of the PlanetScope sensors. Table 2 reported the mean and standard error of the considered predictors (PBs and VIs) in this study during the different phenological stages. The calculated VIs reported different values during the different olive phenological stages. In general, the maximum value was reported for TVI, whereas the minimum was reported for MCARI in both years. Some VIs values did not have a regular trend and changed (with higher or lower values) according to the phenological phase and/or the study year. The NDVI values, for example, show the same trend as the Ψ_{stem} , where the values dropped during the summer period (particularly in July and August) in both study years. Among the calculated VIs, the TVI index gave the highest value, whereas the lowest value was reported for MCARI at the different olive phenological stages and during both seasons.

Table 2. Mean and standard error of the predictors considered in this study (vegetation indices (VIs) and Planet Bands' reflectance (PBs)) during the different phenological stages (mean of 24 sample olive trees) for the two years of the study (2021 and 2022).

2021								
	Fruit Development 10%		Fruit Development 50%		Beginning of Fruit Color		Harvest Maturity	
	Mean	St. Er	Mean	St. Er	Mean	Er.st	Mean	St. Er
B1	0.0473	0.0005	0.0401	0.0005	0.0802	0.0004	0.0309	0.0005
B2	0.0569	0.0005	0.0467	0.0006	0.0500	0.0005	0.0314	0.0005
B3	0.0819	0.0007	0.0766	0.0009	0.1014	0.0004	0.0438	0.0007
B4	0.0940	0.0009	0.0771	0.0010	0.0749	0.0005	0.0562	0.0007
B5	0.1219	0.0010	0.1276	0.0010	0.1392	0.0007	0.0689	0.0010
B6	0.1381	0.0011	0.1169	0.0012	0.1061	0.0009	0.0717	0.0012
B7	0.1665	0.0012	0.1449	0.0013	0.1358	0.0009	0.1017	0.0014
B8	0.2758	0.0016	0.2600	0.0016	0.2772	0.0009	0.2235	0.0021
NDVI	0.4202	0.0034	0.3797	0.0028	0.4467	0.0032	0.5150	0.0048
OSAVI	0.3561	0.0027	0.3091	0.0020	0.3655	0.0024	0.3871	0.0033
TCARI	0.0428	0.0014	0.0334	0.0015	0.0424	0.0013	0.0512	0.0021
TCARI/OSAVI	0.1198	0.0035	0.1078	0.0045	0.1159	0.0031	0.1320	0.0049
EVI	0.2691	0.0023	0.2220	0.0016	0.2781	0.0021	0.2678	0.0027
MCARI	0.0241	0.0009	0.0179	0.0009	0.0226	0.0007	0.0301	0.0016
MCARI/OSAVI	0.4085	0.0034	0.4497	0.0030	0.3826	0.0030	0.3205	0.0042
SR	0.4085	0.0034	0.4497	0.0030	0.3826	0.0030	0.3205	0.0042
TVI	0.9592	0.0018	0.9379	0.0015	0.9729	0.0016	1.0074	0.0024
NDRE	0.3142	0.0024	0.2845	0.0028	0.3424	0.0027	0.3749	0.0043
2022								
	Fruit Development 10%		Fruit Development 50%		Beginning of fruit color		Harvest maturity	
	Mean	St. Er	Mean	St. Er	Mean	Er.st	Mean	St. Er
B1	0.0652	0.0005	0.0617	0.0007	0.0650	0.0007	0.0442	0.0006
B2	0.0463	0.0005	0.0491	0.0007	0.0721	0.0004	0.0387	0.0004
B3	0.0863	0.0006	0.0810	0.0006	0.0794	0.0006	0.0363	0.0005
B4	0.0812	0.0007	0.0853	0.0007	0.0985	0.0007	0.0520	0.0006
B5	0.1289	0.0011	0.1091	0.0007	0.1128	0.0008	0.0535	0.0007
B6	0.1185	0.0011	0.1229	0.0011	0.1314	0.0011	0.0635	0.0008
B7	0.1553	0.0010	0.1586	0.0009	0.1588	0.0012	0.0913	0.0014
B8	0.3042	0.0016	0.2887	0.0013	0.2890	0.0012	0.2093	0.0016
NDVI	0.4394	0.0040	0.4032	0.0033	0.3751	0.0033	0.5348	0.0029
OSAVI	0.3697	0.0033	0.3367	0.0026	0.3151	0.0027	0.3908	0.0020
TCARI	0.0520	0.0016	0.0504	0.0017	0.0385	0.0017	0.0495	0.0016
TCARI/OSAVI	0.1402	0.0035	0.1495	0.0045	0.1219	0.0051	0.1269	0.0042
EVI	0.2784	0.0030	0.2503	0.0023	0.2566	0.0025	0.2803	0.0020
MCARI	0.0289	0.0010	0.0274	0.0011	0.0187	0.0009	0.0289	0.0012
MCARI/OSAVI	0.3898	0.0039	0.4255	0.0034	0.4547	0.0036	0.3032	0.0025
SR	0.3898	0.0039	0.4255	0.0034	0.4547	0.0036	0.3032	0.0025
TVI	0.9692	0.0021	0.9503	0.0017	0.9354	0.0018	1.0172	0.0014
NDRE	0.3242	0.0026	0.2908	0.0024	0.2909	0.0030	0.3930	0.0050

3.3. Evaluation of ψ_{stem} Prediction Performance

3.3.1. Dataset Combination Approach

The following subsections report the results of the models' training conducted after combining the datasets from the two years of the experiment.

Random Forest

The results obtained from the RF-based model were similar to the results obtained using the other modeling approaches when considering VIs as Ψ_{stem} predictors (Testing $R^2 = 0.57$; Testing nRMSE = 18.80%) (Table 3; Figure S2). However, when PBs were used as model predictors, the results significantly improved (Testing $R^2 = 0.78$; Testing nRMSE = 13.20%).

Table 3. Performance of the robustness of the models trained with datasets combination.

Model	Predictors	Calibration				Testing			
		R ²	RMSE	nRMSE	MAE	R ²	RMSE	nRMSE	MAE
RF	VIs	0.92	0.22	6.30%	0.17	0.57	0.55	18.80%	0.38
	PBs	0.90	0.26	7.40%	0.20	0.78	0.38	13.20%	0.28
SVM	VIs	0.66	0.42	13.30%	0.28	0.19	0.58	19.80%	0.46
	PBs	0.82	0.32	11.20%	0.22	0.53	0.52	17.90%	0.40
MLR	VIs	0.54	0.57	15.90%	0.45	0.57	0.55	18.80%	0.44
	PBs	0.76	0.39	13.40%	0.26	0.58	0.49	17.30%	0.40

The optimization of RF model parameters (min node size, mtry, and splitting rule) with PBs as predictors are reported in Figure 4. The importance of the variables is reported in Figure 5. A high percentage of importance indicates that the explanatory variables are an important predictor for the Ψ_{stem} of the olive trees. In this study, the results indicate that B5 (600–620 nm) had the highest value of importance in the model (100%), followed by B4 (547–583 nm), with the second-best value of importance. In contrast, the other PBs had an importance value lower than 40%. The B2 (465–515 nm in the blue region) had no weight of importance in the model.

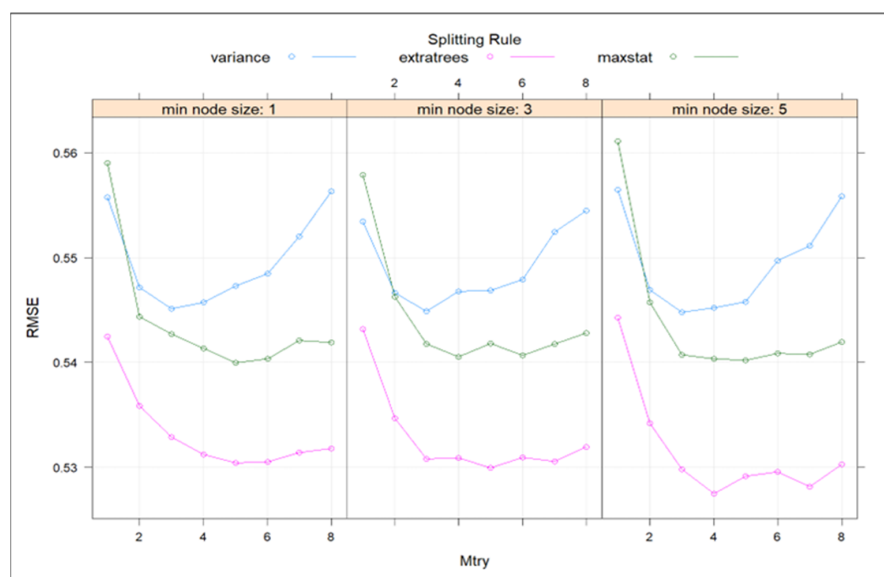


Figure 4. Optimization of RF-based model parameters (min node size; mtry; splitting rule) using PBs as Ψ_{stem} predictors.

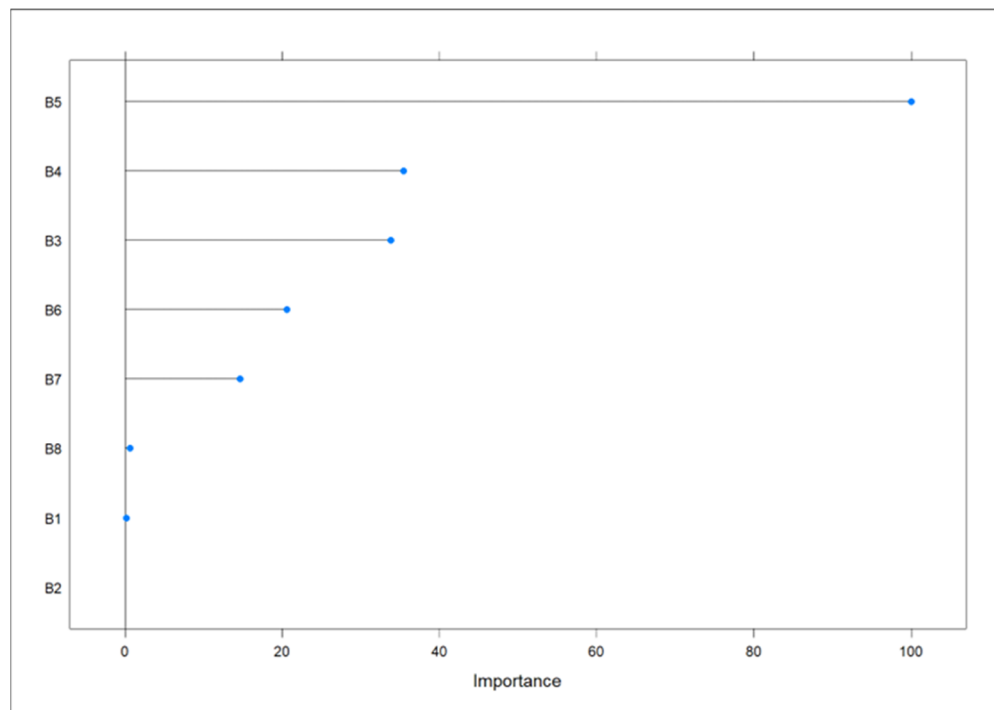


Figure 5. Results of permutation procedure to assess the importance of the variables of the RF-based model using PBs (B1–B8) as predictors of olive Ψ_{stem} .

According to the values of the model performance parameters (R^2 , RMSE, nRMSE, MAE), it is evident that the RF-based model gives more accurate Ψ_{stem} prediction results compared to the MLR and SVM models at both calibration and testing levels (Table 3). In addition, Pearson's correlation (Figure 6) showed a significant correlation between measured Ψ_{stem} and predicted Ψ_{stem} of the RF-based model when the model uses the PBs as predictors. In particular, the correlation between measured and predicted Ψ_{stem} from the calibration dataset was higher ($r = 0.95$) than the correlation from the testing dataset ($r = 0.89$).

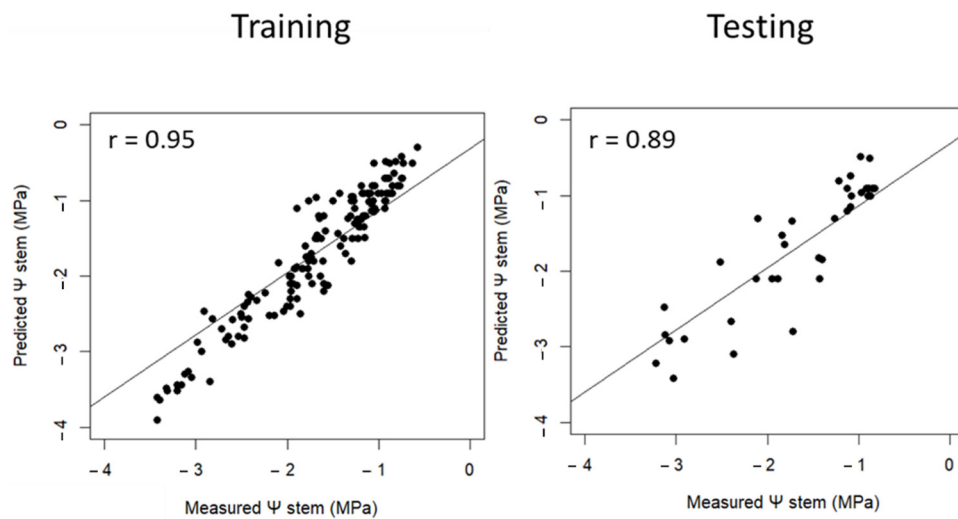


Figure 6. Pearson's correlation between measured and predicted Ψ_{stem} using the RF-based model and PBs as predictors.

Support Vector Machine

The results indicate that the SVM-based model had the lowest accuracy results in predicting olive Ψ_{stem} when compared to other models (Table 3). This was supported by the

Testing R^2 and Testing nRMSE values both when using VIs ($R^2 = 0.19$ and nRMSE = 19.80%) and PBs ($R^2 = 0.53$ and nRMSE = 17.90%) as model predictors (Table 3; Figures S1 and S2).

Multiple Linear Regression

Considering PBs as predictors, the performance results of the MLR-based model are lower than those obtained with RF (MLR: Testing $R^2 = 0.57$; RF: Testing $R^2 = 0.78$) but very similar to those obtained with SVM (MLR: Testing $R^2 = 0.57$; RF: Testing $R^2 = 0.53$) (Table 3; Figures S1 and S2). Considering VIs as predictors, the MLR-based model performed worse than RF. On the contrary, the MLR-based model performed better compared with the results of SVM (MLR: Testing $R^2 = 0.57$; SVM: Testing $R^2 = 0.19$).

Stem Water Potential Predictive Map

Using the RF-based model, a Ψ_{stem} prediction map was produced for each DOY of field measured Ψ_{stem} in both years (Figure 7). The figure shows high-resolution olive Ψ_{stem} prediction maps, using the RF-based model and the PBs as model predictors, at the different olive Ψ_{stem} field measurements. Most of the maps in Figure 7 show a distribution of Ψ_{stem} across the studied olive orchard in both years. Considering the maps of the 2021 season (Figure 7a–d), Ψ_{stem} values appear higher in June than the other three dates. On the contrary, considering the maps of the 2022 season (Figure 7a'–d'), Ψ_{stem} values appear higher in the middle of the season (July and August).

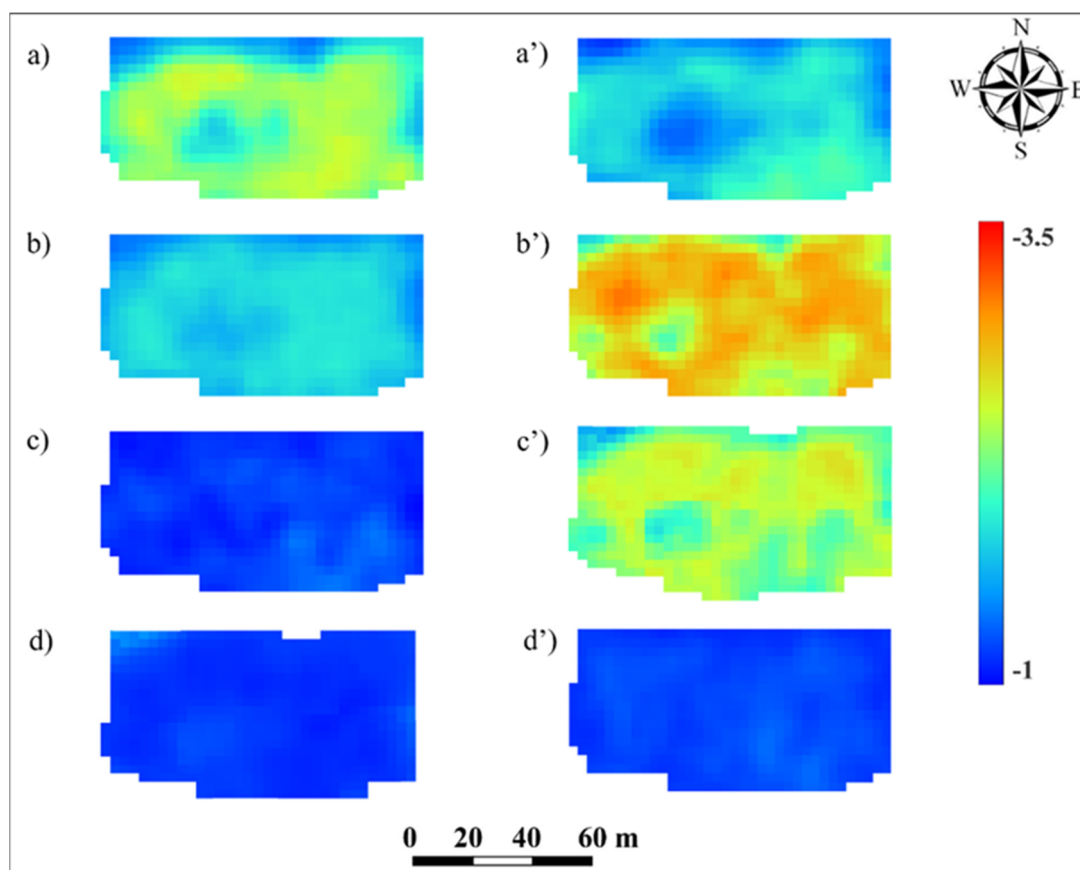


Figure 7. High-resolution Ψ_{stem} prediction maps of the studied olive orchard derived from the RF-based model at the time of SWP measurements during 2021 ((a): DOY 178, (b): DOY 210, (c): DOY 231 and (d): DOY 293) and 2022 ((a'): DOY 164, (b'): DOY 206, (c'): DOY 241 and (d'): DOY 286) seasons.

3.3.2. One-Year Models' Training and Evaluation

The analyses conducted using the second approach (training on the first-year dataset and testing on the second-year dataset) did not lead to notable results. The results of the model training and testing are detailed in Table 4.

Table 4. Performance of the robustness of models trained on the first-year dataset.

Model	Predictors	Calibration				Testing			
		R ²	RMSE	nRMSE	MAE	R ²	RMSE	nRMSE	MAE
RF	PBs	0.72	0.28	12.9	0.21	-0.56	1.29	32.5	0.91
	VI _s	0.67	0.30	13.9	0.23	-0.43	1.08	31.1	0.87
SVM	PBs	-2.74	0.43	60.5	0.32	-130.51	1.23	280.9	0.99
	VI _s	0.75	0.21	11.8	0.12	-51.26	1.89	143.2	0.95
LM	PBs	0.38	0.42	19.2	0.32	-1.10	1.31	37.7	1.01
	VI _s	0.28	0.45	20.7	0.36	-0.44	1.08	31.3	0.88

4. Discussion

In this study, Ψ_{stem} was measured during two irrigation seasons in order to investigate the ability of the proposed prediction models to estimate olive Ψ_{stem} with reasonable accuracy, which can represent an economically viable option for olive growers and help them manage water resources more sustainably. The high variation in Ψ_{stem} (particularly in July and August) is in line with the results found in the literature [8]. Previous studies have highlighted that, as the olive tree is considered a drought-resistant species, a wide range of Ψ_{stem} in olive orchards can be expected under different cultivated conditions [44] and different cultivars [45]. In addition, Giorio et al. [46] highlighted that the olive tree is characterized by low hydraulic conductivity, which can be responsible for a high degree of variation in Ψ_{stem} in response to changing environmental factors [9]. The Ψ_{stem} range reported in this study agreed with the ranges reported by several other studies [47,48] for 'Arbequina' trees. Despite the variation, Ψ_{stem} values lower than -4 MPa were not recorded, perhaps due to some root absorption of water occurring at deeper layers of the soil profile, in line with the result reported by Alcaras et al. [49].

In our study, we did not obtain notable results when the models were trained with the first-year data; this could probably be due to the limited size of the training dataset (the first-year dataset consists of 96 observations) [50]. Hereinafter, the discussion is focused only on the models trained after combining the data from the two experimental years.

Several studies used satellite thermal data to monitor crop water status. However, thermal bands (e.g., bands 10 and 11, Landsat-8) are characterized by low spatial resolution, which could affect the applicability of the model in water status monitoring, particularly in fruit tree crop systems [51]. A review by Ollinger [52] highlighted that the difference in visible vs. NIR reflectance could be significantly related to various properties of plant density or canopy 'greenness'. In this study, we used the full spectral measurements in the VIS, Red Edge, and NIR regions to improve Ψ_{stem} prediction accuracy in olive trees. Rallo et al. [53] indicated that the technological progress in the industrial production of hyperspectral sensors, characterized by a high number of contiguous spectral bands, has driven scientists to a more accurate analysis aimed at selecting specific wavebands that should be more sensitive to crop-related variables [54,55]. For example, using hyperspectral imagery, Zarco-Tejada et al. [56] demonstrated the ability of a VI, centered at 570 and 515 nm wavelengths, as a water stress indicator. Various studies have considered the full spectral information on the basis of multivariate statistical techniques to take advantage of an increased number of wavebands and to improve the prediction of crop-related parameters [53,57]; however, little research has considered PBs and VIs independently as model predictors in order to improve the model prediction accuracy. RF, SVM, and MLR were previously used [41] to predict the canopy nitrogen weight from individual multispectral bands and associated vegetation indices (VI). The authors found that both

machine-learning models provided much better accuracy than linear regression. Regarding water status estimation, however, very few studies have been carried out on the applicability of machine learning techniques such as SVM and RF in determining crop water stress in different crops [58] using multispectral remote sensing data.

These results show that the RF-based model, using PBs as predictors, is a good machine-learning technique to estimate Ψ_{stem} in the olive orchard using Planet satellite data. In fact, as it becomes easier to implement artificial intelligence algorithms, more and more studies focus on the use of machine learning that uses all available spectral bands [59], taking into account all the information included in the spectra [59,60]. Our findings suggest that the most important PBs to predict Ψ_{stem} with an RF-based model were B5 and B4. The high-importance variable found for B5 could be explained by alterations in leaf characteristics due to the water stress that could determine changes in optical properties in the specific spectral range of 600–620 nm. Carter et al. [61] reported that leaf dehydration could determine a change in the spectral response of the leaf around the yellow region. Furthermore, a vegetation index (Yellowness Index) was reported in the literature that was developed to assess chlorosis in stressed leaves by evaluating how the reflectance changes around 600 nm [62]. It should be taken into account that drought stress and the consequent reduction of water in the tissues reduce cell turgor and could lead to photosystem damage and chlorosis [63,64]. The findings related to the importance of the variables are specific to our study, field conditions, cultivar, and RF-modeling approach. Thus, they cannot be generalized; moreover, further research is needed to confirm or deny our findings. According to the authors' knowledge, there have been no attempts in the literature to develop a reliable prediction model for the estimation of water status in terms of Ψ_{stem} in olive orchards using spectral bands and vegetation indices as model predictors through the machine learning technique. Nevertheless, this modeling approach has been widely used for the estimation of water status in other tree crops. In vineyards, for example, a study by Rienth and Scholasch [65] relied on a relationship between VI (e.g., NDVI) and crop coefficients to predict crop water status. In contrast, other studies [66,67] highlighted that VI with red edge (RE) and shortwave infrared (SWIR) positions are more related to crop water status. In agreement with our findings, several studies on vineyards [59,60] have suggested that machine learning techniques can provide more accurate results in predicting crop water status in terms of Ψ_{stem} when using single bands instead of VIs. In particular, the study of Laroche-Pinel et al. [59] tested five machine-learning algorithms to find possible relationships between stem water potential and data acquired from Sentinel-2 images (bands reflectance values and vegetation indices). The authors found that when using red, NIR, red edge, and SWIR bands, the regression model gave promising results in predicting Ψ_{stem} ($R^2 = 0.40$, RMSE = 0.26) in vineyards. However, sentinel-2 has some disadvantages compared to Planet, including lower spatial and temporal resolution (Planet provides daily images [24]).

The RF algorithm is a widely used machine learning approach to highlight non-linear relationships between predictor variables [67]. Such a model is well suited for natural and biological phenomena that are complex and non-linear [68]. However, the choice of predictors is essential. In our modeling approach, using VIs as predictors, the performance was lower than the one using PBs. The RF algorithm was probably able to identify different and better relationships between the bands for the Ψ_{stem} prediction compared to linear relationships identified by well-known VIs [69]. In this study, another commonly used machine learning model, SVM, was applied to test its ability to predict olive Ψ_{stem} despite the advantage of the SVM modeling approach due to its ability to successfully handle small training data sets with only a few samples [70]. In our study, SVM had the worst performance compared to RF and MLR. The results suggest that the SVM-based model is not sufficiently acceptable for predicting Ψ_{stem} using images acquired by PSB.SD. A previous study by Fernandes et al. [71] indicates that the use of the SVM method for water stress detection in olives implies some assumptions, such as data normality, and requires that independent variables are identically distributed, thus reducing their applicability.

In agreement with the results of this work, Pôças et al. [72] selected three hyperspectral reflectance vegetation indices (NIR, WI, and D1) and the DOY as predictors for the inclusion in RF and SVM predictive machine learning models for assessing water stress in grapevines. The authors found that the RF-based model gave the best water stress prediction results ($R^2 = 0.77$) compared to SVM ($R^2 = 0.71$). Furthermore, a recent review of support vector machines in precision agriculture [73] indicates that SVM had better performance, both for classification and regression problems, than other machine learning techniques except for RF, in line with the results of our study.

The imaging tools provide technicians and researchers the opportunity to better examine and understand spatial and temporal variability through the use of maps [74]. Maps can be obtained using vegetation indices, a linear combination of a certain number of bands, and so on [75], or, as in the case of this study, considering a particular parameter predicted through a machine learning technique. Pearson's correlation of the RF-based model data and the PBs as model predictors showed a high correlation between measured and predicted Ψ_{stem} for the calibration dataset ($r = 0.95$), whereas, for the testing dataset, a slightly lower correlation was obtained ($r = 0.89$). The prediction maps indicate that the RF-based model was able to reproduce the spatial variability of Ψ_{stem} close to field measured Ψ_{stem} . The maps show a wide spatial variability within the olive orchard, particularly due to the absence of olive trees in specific portions of the field. Moreover, it should be taken into account that other factors could influence the spectral response within each pixel, e.g., soil management and weed communities' composition. Borgogno-Mondino et al. [76] obtained Ψ_{stem} maps of a pomegranate orchard using Sentinel-2 images. The maps obtained in this work have the advantage of a better spatial resolution (3 m per pixel). In fact, a limitation in the use of satellites in agriculture could be due to the low resolution of the images [32].

5. Conclusions

The lack of a time-saving and reliable remote sensing methodology for the estimation of crop water status in olive orchards inspired us to develop a practical solution for the reasonable estimation of Ψ_{stem} that can avoid expensive and time-consuming fieldwork within the framework of precision management of irrigation water. We used Planet reflectance data and measured Ψ_{stem} data from 24 olive trees to derive a Ψ_{stem} prediction model for in-season estimation of Ψ_{stem} at the olive orchard.

Our study found that the random forest (RF)-based modeling approach using PBs as predictors can provide a more accurate Ψ_{stem} prediction compared with SVM and MLR. The variable importance found in RF modeling suggests that the yellow and green spectral regions (B5 and B4, respectively) were the most important in Ψ_{stem} prediction. However, our findings are specific and related to the field conditions and, therefore, need to be confirmed by further and long-term studies.

This is the first study to combine machine learning techniques and high-resolution satellite data for the development of a reliable prediction model of water status in olive orchards. Our findings can help farmers and technicians monitor the variability of olive water status during the irrigation season for better water irrigation management. Our study demonstrates the feasibility of using satellite multispectral imagery and machine learning to create a semi-automated olive water stress modeling framework. However, these results are site-specific, and further studies are needed to test the temporal and spatial prediction accuracy.

Our results open the door for deeper studies in which our models can be integrated with other agrometeorological information and used to implement more complex algorithms and software that can support farmers in water irrigation management in olive orchards (e.g., decision support systems).

Supplementary Materials: The following supporting information can be downloaded at <https://www.mdpi.com/article/10.3390/agronomy14010001/s1>. Figure S1: Pearson's correlation between measured and predicted Ψ_{stem} using the random forest-based model (a), support vector machine (b) and linear model (c) with Planet spectral bands as predictors; Figure S2: Pearson's correlation between measured and predicted Ψ_{stem} using the random forest-based model (a), support vector machine (b) and linear model (c) with vegetation indices as predictors; Table S1: The amount of irrigation water applied prior to the date of stem water potential (Ψ_{stem}) measurement and the number of days prior to stem water potential measurement date on which rainfall occurred, in both the irrigation seasons considered; Table S2: Monthly irrigation water applied and monthly rainfall in both the irrigation seasons considered; Table S3: The amount of water applied per each date of irrigation during both the irrigation seasons considered.

Author Contributions: Conceptualization, V.G. and G.A.V.; data curation, S.P.G., S.A.A., F.P.S. and G.A.V.; formal analysis, S.P.G., V.G. and L.C.; funding acquisition, G.A.V.; investigation, S.P.G., L.C. and G.L.; methodology, V.G. and G.A.V.; project administration, G.A.V.; resources, G.A.V.; software, S.P.G.; supervision, G.A.V.; validation, G.A.V.; visualization, S.P.G.; writing—original draft, S.P.G.; writing—review & editing, V.G., L.C., S.A.A., S.C., G.L., F.P.S. and G.A.V. All authors have read and agreed to the published version of the manuscript.

Funding: This study was carried out within the Agritech National Research Center and received funding from the European Union NextGenerationEU (PIANO NAZIONALE DI RIPRESA E RESILIENZA (PNRR)—MISSIONE 4 COMPONENTE 2, INVESTIMENTO 1.4—D.D. 1032 17/06/2022, CN00000022). This manuscript reflects only the authors' views and opinions. Neither the European Union nor the European Commission can be considered responsible for them.

Data Availability Statement: Data are available upon request.

Acknowledgments: The authors thank Planet Labs PBC for providing images as part of Planet's Education and Research Program.

Conflicts of Interest: The authors declare that they have no known competing financial interest or personal relationships that could have appeared to influence the work reported in this paper.

References

1. Kostelenos, G.; Kiritsakis, A. Olive tree history and evolution. In *Olives and Olive Oil as Functional Foods: Bioactivity, Chemistry and Processing*; John Wiley & Sons, Ltd.: Hoboken, NJ, USA, 2017; pp. 1–12. [[CrossRef](#)]
2. Uylâsler, V.; Yıldız, G. The historical development and nutritional importance of olive and olive oil constituted an important part of the Mediterranean diet. *Crit. Rev. Food Sci. Nutr.* **2014**, *54*, 1092–1101. [[CrossRef](#)] [[PubMed](#)]
3. Grigg, D. Olive oil, the Mediterranean and the world. *GeoJournal* **2001**, *53*, 163–172. [[CrossRef](#)]
4. IOOC. International Olive Oil Council. 2011. Available online: <http://www.internationaloliveoil.org/noticias> (accessed on 15 February 2023).
5. Scorticchini, M. The Multi-Millennial Olive Agroecosystem of Salento (Apulia, Italy) Threatened by *Xylella Fastidiosa* Subsp *Pauca*: A Working Possibility of Restoration. *Sustainability* **2020**, *12*, 6700. [[CrossRef](#)]
6. Loumou, A.; Giourga, C. Olive groves: The life and identity of the Mediterranean. *Agric. Hum. Values* **2003**, *20*, 87–95. [[CrossRef](#)]
7. Orgaz, F.; Fereres, E. Viability in Adaptative Mechanisms to Water Deficits in Annual and Perennial Crop Plants. *Bull. Société Bot. Fr. Actual. Bot.* **1984**, *131*, 17–32. [[CrossRef](#)]
8. Sepulcre-Cantó, G.; Zarco-Tejada, P.J.; Jiménez-Muñoz, J.C.; Sobrino, J.A.; De Miguel, E.; Villalobos, F.J. Detection of water stress in an olive orchard with thermal remote sensing imagery. *Agric. For. Meteorol.* **2006**, *136*, 31–44. [[CrossRef](#)]
9. Lopriore, G.; Tarantino, A. Irrigation of intensive olive groves in the Mediterranean environment with different water regimes on two different soils: Effects on carpological parameters and technological and qualitative characteristics of the oils. *Acta Hortic.* **2022**, *1335*, 549–556. [[CrossRef](#)]
10. Romero-Trigueros, C.; Vivaldi, G.A.; Nicolás, E.N.; Paduano, A.; Salcedo, F.P.; Camposeo, S. Ripening Indices, Olive Yield and Oil Quality in Response to Irrigation With Saline Reclaimed Water and Deficit Strategies. *Front. Plant Sci.* **2019**, *10*, 1243. [[CrossRef](#)]
11. Scalisi, A.; Marino, G.; Marra, F.P.; Caruso, T.; Lo Bianco, R. A Cultivar-Sensitive Approach for the Continuous Monitoring of Olive (*Olea europaea* L.) Tree Water Status by Fruit and Leaf Sensing. *Front. Plant Sci.* **2020**, *11*, 340. [[CrossRef](#)]
12. Pinter, P.J., Jr.; Hatfield, J.L.; Schepers, J.S.; Barnes, E.M.; Moran, M.S.; Daughtry, C.S.T.; Upchurch, D.R. Remote sensing for crop management. *Photogramm. Eng. Remote Sensing* **2003**, *69*, 647–664. [[CrossRef](#)]
13. Govender, M.; Dye, P.J.; Weiersbye, I.M.; Witkowski, E.T.F.; Ahmed, F. Review of commonly used remote sensing and ground-based technologies to measure plant water stress. *Water SA* **2009**, *35*, 741–752. [[CrossRef](#)]

14. Dzikiti, S.; Verreyne, J.S.; Stuckens, J.; Strever, A.; Verstraeten, W.W.; Swennen, R.; Coppin, P. Determining the water status of Satsuma mandarin trees [Citrus Unshiu Marcovitch] using spectral indices and by combining hyperspectral and physiological data. *Agric. For. Meteorol.* **2010**, *150*, 369–379. [[CrossRef](#)]
15. McCutchan, H.; Shackel, K.A. Stem-water Potential as a Sensitive Indicator of Water Stress in Prune Trees (*Prunus domestica* L. cv. French). *J. Am. Soc. Hortic. Sci.* **1992**, *117*, 607–611. [[CrossRef](#)]
16. Naor, A.; Gal, Y.; Peres, M. The inherent variability of water stress indicators in apple, nectarine and pear orchards, and the validity of a leaf-selection procedure for water potential measurements. *Irrigation Sci.* **2006**, *8*, 129–135. [[CrossRef](#)]
17. Suárez, L.; Zarco-Tejada, P.J.; Berni, J.A.J.; González-Dugo, V.; Fereres, E. August. Orchard Water Stress detection using high-resolution imagery. *Acta Hortic.* **2011**, *922*, 35–39. [[CrossRef](#)]
18. Caruso, G.; Palai, G.; Tozzini, L.; Gucci, R. Using VIstable and Thermal Images by an Unmanned Aerial Vehicle to Monitor the Plant Water Status, Canopy Growth and Yield of Olive Trees (cvs. Frantoio and Leccino) under Different Irrigation Regimes. *Agronomy* **2022**, *12*, 1904. [[CrossRef](#)]
19. Ahumada-Orellana, L.E.; Ortega-Farías, S.; Searles, P.S.; Retamales, J.B. Yield and water productivity responses to irrigation cut-off strategies after fruit set using stem water potential thresholds in a super-high density olive orchard. *Front. Plant Sci.* **2017**, *8*, 1280. [[CrossRef](#)]
20. Lopriore, G.; Caliandro, A. Irrigation of intensive olive groves in the Mediterranean environment with different water regimes on two different soils: Effects on yields, water use efficiency, vegetative behaviour and water status of the crop. *Acta Hortic.* **2022**, *1335*, 541–548. [[CrossRef](#)]
21. Lopriore, G.; Gatta, G.; Scelsa, D.; Lo Storto, M.C.; Abatantuono, I.A.; Pati, S. Water Stress, Yield and Oil Characteristics Of PRD And Deficit Irrigated Very-High Density Olive Orchard (*Olea europaea* L. cv. ‘Arbequina’). *Acta Hortic.* **2016**, *1112*, 87–94. [[CrossRef](#)]
22. Caruso, G.; Zarco-Tejada, P.J.; González-Dugo, V.; Moriondo, M.; Tozzini, L.; Palai, G.; Rallo, G.; Hornero, A.; Primicerio, J.; Gucci, R. High-resolution imagery acquired from an unmanned platform to estimate biophysical and geometrical parameters of olive trees under different irrigation regimes. *PLoS ONE* **2019**, *14*, e0210804. [[CrossRef](#)]
23. Suárez, L.; Zarco-Tejada, P.J.; Sepulcre-Cantó, G.; Pérez-Priego, O.; Miller, J.R.; Jiménez-Muñoz, J.C.; Sobrino, J. Assessing canopy PRI for water stress detection with diurnal airborne imagery. *Remote Sens. Environ.* **2008**, *112*, 560–575. [[CrossRef](#)]
24. Planet Imagery Product Specifications. 2022. Available online: <https://www.planet.com/products/planet-imagery/> (accessed on 23 January 2023).
25. QGIS.org. QGIS Geographic Information System. QGIS Association. 2023. Available online: <http://www.qgis.org> (accessed on 31 March 2023).
26. Regione Puglia—Disciplinare di Produzione Integrata—Anno 2020. Legge Regionale n. n. 22 del 20 Febbraio 2020, 11, Bollettino Ufficiale della Regione Puglia (Guidelines for the Sustainable Crop Production of the Apulian Region). Available online: <https://www.regione.puglia.it/documents/42866/197836/Disciplinare+Produzione+Integrata++Sezione+Agronomica+-+2020.pdf/a0218c6a-c24e-31fc-4f3e-2add98fcf64c?t=1585737261315> (accessed on 3 March 2023).
27. Climate Data. 2023. Available online: <https://it.climate-data.org/europa/italia/puglia/gallipoli-14072/> (accessed on 23 January 2023).
28. Regione Puglia. Available online: <https://protezionecivile.puglia.it/rete-di-monitoraggio-e-dati-meteo-idrometrici> (accessed on 23 January 2023).
29. Hargreaves, G.H.; Samani, Z.A. Reference crop evapotranspiration from temperature. *Appl. Eng. Agric.* **1985**, *1*, 96–99. [[CrossRef](#)]
30. Pedrero, F.; Grattan, S.; Ben-Gal, A.; Vivaldi, G.A. Opportunities for expanding the use of wastewaters for irrigation of olives. *Agric. Water Manag.* **2020**, *241*, 106333. [[CrossRef](#)]
31. Frazier, A.E.; Hemingway, B.L. A technical review of planet smallsat data: Practical considerations for processing and using planetscope imagery. *Remote Sens.* **2021**, *13*, 3930. [[CrossRef](#)]
32. Mazzia, V.; Comba, L.; Khalil, A.; Chiaberge, M.; Gay, P. UAV and Machine Learning Based Refinement of a Satellite-Driven Vegetation Index for Precision Agriculture. *Sensors* **2020**, *20*, 2530. [[CrossRef](#)]
33. Rouse, W.; Haas, R.H.; Deering, D.W. Monitoring Vegetation Systems in the Great Plains with ERTS; Third ERTS Symposium (NASA SP-351); NASA: Washington, DC, USA, 1974; Volume 1.
34. Rondeaux, G.; Steven, M.; Baret, F. Optimization of soil-adjusted vegetation indices. 1996. *Remote Sens. Environ.* **1996**, *55*, 95–107. [[CrossRef](#)]
35. Daughtry, C.S.T.; Walthall, C.L.; Kim, M.S.; De Colstoun, E.B.; McMurtrey, J.E., III. Estimating corn leaf chlorophyll concentration from leaf and canopy reflectance. *Remote Sens. Environ.* **2000**, *74*, 229–239. [[CrossRef](#)]
36. Haboudane, D.; Miller, J.R.; Tremblay, N.; Zarco-Tejada, P.J.; Dextraze, L. Integrating hyperspectral vegetation indices for accurate predictions of crop chlorophyll content for application to precision agriculture. *Remote Sens. Environ.* **2002**, *81*, 416–426. [[CrossRef](#)]
37. Huete, A.; Didan, K.; Miura, T.; Rodriguez, E.P.; Gao, X.; Ferreira, L.G. Overview of the radiometric and biophysical performance of the MODIS vegetation indices. *Remote Sens. Environ.* **2002**, *83*, 195–213. [[CrossRef](#)]
38. Huete, A.; Justice, C.; Liu, H. Development of vegetation and soil indices for MODIS-EOS. *Remote Sens. Environ.* **1994**, *49*, 224–234. [[CrossRef](#)]
39. Bannari, A.; Morin, D.; Bonn, F.; Huete, A.R. A review of vegetation indices. *Remote Sens. Rev.* **1995**, *13*, 95–120. [[CrossRef](#)]

40. Gareth, J.; Daniela, W.; Trevor, H.; Robert, T. *An Introduction to Statistical Learning: With Applications in R*; Springer: New York, NY, USA, 2013; p. 18.
41. Lee, H.; Wang, J.; Leblon, B. Using Linear Regression, Random Forests, and Support Vector Machine with Unmanned Aerial Vehicle Multispectral Images to Predict Canopy Nitrogen Weight in Corn. *Remote Sens.* **2020**, *12*, 2071. [[CrossRef](#)]
42. Liu, Y.; Wang, Y.; Zhang, J. New Machine Learning Algorithm: Random Forest. *Lect. Notes Comput. Sci.* **2012**, *7473*, 246–252. [[CrossRef](#)]
43. Janitza, S.; Strobl, C.; Boulesteix, A.L. An AUC-based permutation variable importance measure for random forests. *BMC Bioinform.* **2013**, *14*, 119. [[CrossRef](#)] [[PubMed](#)]
44. Shackel, K.; Moriana, A.; Marino, G.; Corell, M.; Pérez-López, D.; Martín-Palomo, M.J.; Caruso, T.; Marra, F.P.; Agüero Alcaras, L.M.; Milliron, L.; et al. Establishing a reference baseline for midday stem water potential in olive and its use for plant-based irrigation management. *Front. Plant Sci.* **2021**, *12*, 791711. [[CrossRef](#)] [[PubMed](#)]
45. Marino, G.; Pernice, F.; Marra, F.P.; Caruso, T. Validation of an online system for the continuous monitoring of tree water status for sustainable irrigation managements in olive (*Olea europaea* L.). *Agric. Water Manag.* **2016**, *177*, 298–307. [[CrossRef](#)]
46. Giorio, P.; Sorrentino, G.; d’Andria, R. Stomatal behaviour, leaf water status and photosynthetic response in field-grown olive trees under water deficit. *Environ. Exp. Bot.* **1999**, *42*, 95–104. [[CrossRef](#)]
47. Fernández, J.E.; Rodríguez-Domínguez, C.M.; Perez-Martin, A.; Zimmermann, U.; Rüger, S.; Martín-Palomo, M.J.; Torres-Ruiz, J.M.; Cuevas, M.V.; Sann, C.; Ehrenberger, W.; et al. Online-monitoring of tree water stress in a hedgerow olive orchard using the leaf patch clamp pressure probe. *Agric. Water Manag.* **2011**, *100*, 25–35. [[CrossRef](#)]
48. Ehrenberger, W.; Rüger, S.; Rodríguez-Domínguez, C.M.; Díaz-Espejo, A.; Fernández, J.E.; Moreno, J.; Zimmermann, D.; Sukhorukov, V.L.; Zimmermann, U. Leaf patch clamp pressure probe measurements on olive leaves in a nearly turgorless state. *Plant Biol.* **2012**, *14*, 666–674. [[CrossRef](#)]
49. Alcaras, L.M.A.; Rousseaux, M.C.; Searles, P.S. Responses of several soil and plant indicators to post-harvest regulated deficit irrigation in olive trees and their potential for irrigation scheduling. *Agric. Water Manag.* **2016**, *171*, 10–20. [[CrossRef](#)]
50. Catal, C.; Diri, B. Investigating the Effect of Dataset Size, Metrics Sets, and Feature Selection Techniques on Software Fault Prediction Problem. *Inf. Sci.* **2009**, *179*, 1040–1058. [[CrossRef](#)]
51. Gerhards, M.; Schlerf, M.; Mallick, K.; Udelhoven, T. Challenges and Future Perspectives of Multi-/Hyperspectral Thermal Infrared Remote Sensing for Crop Water-Stress Detection: A Review. *Remote Sens.* **2019**, *11*, 1240. [[CrossRef](#)]
52. Ollinger, S.V. Sources of variability in canopy reflectance and the convergent properties of plants. *New Phytol.* **2011**, *189*, 375–394. [[CrossRef](#)]
53. Rallo, G.; Minacapilli, M.; Ciraolo, G.; Provenzano, G. Detecting crop water status in mature olive groves using vegetation spectral measurements. *Biosyst. Eng.* **2014**, *128*, 52–68. [[CrossRef](#)]
54. Goel, P.K.; Prasher, S.O.; Landry, J.A.; Patel, R.M.; Viau, A.A.; Miller, J.R. Estimation of crop biophysical parameters through airborne and field hyperspectral remote sensing. *Trans. ASAE* **2003**, *46*, 1235. [[CrossRef](#)]
55. Darvishzadeh, R.; Skidmore, A.; Schlerf, M.; Atzberger, C.; Corsi, F.; Cho, M. LAI and chlorophyll estimation for a heterogeneous grassland using hyperspectral measurements. *Int. J. Photogramm. Remote Sens.* **2008**, *63*, 409–426. [[CrossRef](#)]
56. Zarco-Tejada, P.J.; González-Dugo, V.; Williams, L.E.; Suarez, L.; Berni, J.A.; Goldhamer, D.; Fereres, E. A PRI-based water stress index combining structural and chlorophyll effects: Assessment using diurnal narrow-band airborne imagery and the CWSI thermal index. *Remote Sens. Environ.* **2013**, *138*, 38–50. [[CrossRef](#)]
57. Hansen, P.M.; Schjoerring, J.K. Reflectance measurement of canopy biomass and nitrogen status in wheat crops using normalized difference vegetation indices and partial least squares regression. *Remote Sens. Environ.* **2003**, *86*, 542–553. [[CrossRef](#)]
58. Virnodkar, S.S.; Pachghare, V.K.; Patil, V.C.; Jha, S.K. Remote sensing and machine learning for crop water stress determination in various crops: A critical review. *Precis. Agric.* **2020**, *21*, 1121–1155. [[CrossRef](#)]
59. Laroche-Pinel, E.; Duthoit, S.; Albughdadi, M.; Costard, A.D.; Rousseau, J.; Cheret, V.; Clenet, H. Towards vine water status monitoring on a large scale using sentinel-2 images. *Remote Sens.* **2021**, *13*, 1837. [[CrossRef](#)]
60. Loggenberg, K.; Strever, A.; Greyling, B.; Poona, N. Modelling water stress in a Shiraz vineyard using hyperspectral imaging and machine learning. *Remote Sens.* **2018**, *10*, 202. [[CrossRef](#)]
61. Carter, G.A. Responses of Leaf Spectral Reflectance to Plant Stress. *Am. J. Bot.* **1993**, *80*, 239–243. [[CrossRef](#)]
62. Richardson, A.D.; Duigan, S.P.; Berlyn, G.P. An evaluation of noninvasive methods to estimate foliar chlorophyll content. *New Phytol.* **2002**, *153*, 185–194. [[CrossRef](#)]
63. Sanzani, S.M.; Schena, L.; Nigro, F.; Sergeeva, V.; Ippolito, A.; Salerno, M.G. Abiotic Diseases of Olive. *J. Plant Pathol.* **2012**, *94*, 469–491. Available online: <http://www.jstor.org/stable/45156275> (accessed on 30 April 2023).
64. Olorunwa, O.J.; Shi, A.; Barickman, T.C. Varying drought stress induces morpho-physiological changes in cowpea (*Vigna unguiculata* (L.) genotypes inoculated with *Bradyrhizobium japonicum*. *Plant Stress* **2021**, *2*, 100033. [[CrossRef](#)]
65. Rienth, M.; Scholasch, T. State-of-the-art of tools and methods to assess vine water status. *OENO One* **2019**, *53*, 639–659. [[CrossRef](#)]
66. Cohen, Y.; Gogumalla, P.; Bahat, I.; Netzer, Y.; Ben-Gal, A.; Lenski, I.; Michael, Y.; Helman, D. Can time series of multispectral satellite images be used to estimate stem water potential in vineyards? In *Precision Agriculture*; Wageningen Academic Publishers: Wageningen, The Netherlands, 2019; Volume 19, pp. 445–451. [[CrossRef](#)]
67. Romero, M.; Luo, Y.; Su, B.; Fuentes, S. Vineyard water status estimation using multispectral imagery from an UAV platform and machine learning algorithms for irrigation scheduling management. *Comput. Electron. Agric.* **2018**, *147*, 109–117. [[CrossRef](#)]

68. Smith, P.F.; Ganesh, S.; Liu, P. A comparison of random forest regression and multiple linear regression for prediction in neuroscience. *J. Neurosci. Methods* **2013**, *220*, 85–91. [[CrossRef](#)]
69. Arbia, G.; Griffith, D.A.; Haining, R.P. Spatial error propagation when computing linear combinations of spectral bands: The case of vegetation indices. *Environ. Ecol. Stat.* **2003**, *10*, 375–396. [[CrossRef](#)]
70. Mountrakis, G.; Im, J.; Ogole, C. Support vector machines in remote sensing: A review. *ISPRS J. Photogramm. Remote Sens.* **2011**, *66*, 247–259. [[CrossRef](#)]
71. Fernandes, R.D.M.; Cuevas, M.V.; Hernandez-Santana, V.; Rodriguez-Dominguez, C.M.; Padilla-Díaz, C.M.; Fernández, J.E. Classification models for automatic identification of daily states from leaf turgor related measurements in olive. *Comput. Electron. Agric.* **2017**, *142*, 181–189. [[CrossRef](#)]
72. Pôças, I.; Gonçalves, J.; Costa, P.M.; Gonçalves, I.; Pereira, L.S.; Cunha, M. Hyperspectral-based predictive modelling of grapevine water status in the Portuguese Douro wine region. *Int. J. Appl. Earth Obs. Geoinf.* **2017**, *58*, 177–190. [[CrossRef](#)]
73. Kok, Z.H.; Shariff, A.R.M.; Alfatni, M.S.M.; Khairunniza-Bejo, S. Support Vector Machine in Precision Agriculture: A review. *Comput. Electron. Agric.* **2021**, *191*, 106546. [[CrossRef](#)]
74. Lelong, C.C.; Pinet, P.C.; Poilv  , H. Hyperspectral Imaging and Stress Mapping in Agriculture: A Case Study on Wheat in Beauce (France). *Remote Sens. Environ.* **1998**, *66*, 179–191. [[CrossRef](#)]
75. Baret, F.; Guyot, G. Potentials and limits of vegetation indices for LAI and APAR assessment. *Remote Sens. Environ.* **1991**, *35*, 161–173. [[CrossRef](#)]
76. Borgogno-Mondino, E.; Farbo, A.; Novello, V.; de Palma, L. A Fast Regression-Based Approach to Map Water Status of Pomegranate Orchards with Sentinel 2 Data. *Horticulturae* **2022**, *8*, 759. [[CrossRef](#)]

Disclaimer/Publisher’s Note: The statements, opinions and data contained in all publications are solely those of the individual author(s) and contributor(s) and not of MDPI and/or the editor(s). MDPI and/or the editor(s) disclaim responsibility for any injury to people or property resulting from any ideas, methods, instructions or products referred to in the content.